Higher-Order Aberrations Due to the Posterior Corneal Surface in Patients with Keratoconus

Tomoya Nakagawa,[1] *Naoyuki Maeda,*[1] *Ryo Kosaki,*[1] *Yuichi Hori,*[1] *Tomoyuki Inoue,*[1] *Makoto Saika,*[2] *Toshifumi Mihashi,*[2] *Takashi Fujikado,*[1,3] *and Yasuo Tano*[1]

Purpose. This study was designed to investigate higher-order aberrations (HOAs) due to the posterior corneal surface in keratoconic eyes compared with normal eyes.

Methods. We studied 24 normal and 28 keratoconic eyes. The anterior/posterior corneal heights and pachymetric data were obtained with a rotating Scheimpflug camera. HOAs for 6 mm pupils were calculated from the differences between the height data and the best-fit sphere, using an original program for each corneal surface. The reference axes of the measurements were aligned with the primary line of sight. The HOAs were expanded with normalized Zernike polynomials. For each pair of standard Zernike terms for trefoil, coma, tetrafoil, and secondary astigmatism, one value for the magnitude and axis was calculated by Zernike vector analysis.

Results. The mean total corneal HOAs (root mean square [μm]) from the anterior/posterior surfaces were significantly ($P < 0.001$) higher in keratoconic (4.34/1.09, respectively) than in control eyes (0.46/0.15). The mean magnitude of each Zernike vector terms for trefoil, coma, and spherical aberration from the anterior/posterior surfaces was significantly ($P < 0.001$) higher in keratoconic (0.77/0.19, 3.57/0.87, −0.44/0.17) than control eyes (0.09/0.04, 0.33/0.07, 0.25/−0.07), respectively. The mean axes by vector calculation for coma due to the anterior (63.6°) and posterior surfaces (241.9°) were in opposite directions.

Conclusions. Corneal HOAs on both corneal surfaces in keratoconic eyes were higher than in control eyes. Coma from the posterior surface compensated partly for that from the anterior surface. Residual irregular astigmatism in patients with keratoconus wearing rigid gas permeable contact lenses can be estimated by measuring the HOA from the posterior corneal surface. (*Invest Ophthalmol Vis Sci.* 2009;50:2660–2665) DOI: 10.1167/iovs.08-2754

From the Departments of [1]Ophthalmology and [3]Applied Visual Science, Osaka University Medical School, Osaka, Japan; and the [2]Research Institute, Optics Laboratory, Topcon Corporation, Tokyo, Japan.

Supported in part by Grant 18591919 from the Japanese Ministry of Education, Science, Sports, and Culture, Tokyo, Japan.

Submitted for publication August 20, 2008; revised October 17 and November 6, 2008; accepted March 26, 2009.

Disclosure: **T. Nakagawa**, None; **N. Maeda**, None; **R. Kosaki**, None; **Y. Hori**, None; **T. Inoue**, None; **M. Saika**, Topcon Corporation (E); **T. Mihashi**, Topcon Corporation (E); **T. Fujikado**, None; **Y. Tano**, None

Presented in part at the annual meeting of the Association for Research in Vision and Ophthalmology, Fort Lauderdale, Florida, April 2008.

The publication costs of this article were defrayed in part by page charge payment. This article must therefore be marked "*advertisement*" in accordance with 18 U.S.C. §1734 solely to indicate this fact.

Corresponding author: Naoyuki Maeda, Department of Ophthalmology, Osaka University Medical School, Room E7, 2-2 Yamadaoka, Suita, 565-0871, Japan; nmaeda@ophthal.med.osaka-u.ac.jp.

Keratoconus is a corneal disorder characterized by progressive corneal thinning and protrusion. Asymmetric corneal protrusion induces irregular astigmatism leading to impaired visual function.[1,2] Many previous studies have evaluated the deformity and effect on the optical performance of the keratoconic eyes. The typical topographic finding of keratoconus is abnormal localized steepening.[3–6]

The irregular astigmatic component extracted from the topographic data of the corneal anterior surface was significantly correlated with the best spectacle-corrected visual acuity in keratoconic eyes.[7,8] Higher-order aberrations (HOAs) in keratoconic eyes also have been evaluated previously. Wavefront sensing showed significantly larger HOAs in refraction, especially coma-like aberrations, in keratoconic eyes.[9,10] The corneal HOAs calculated from the corneal anterior surface topographic data and the keratometric refractive index in keratoconus also had similar results.[9,11–16]

Rigid gas permeable (RGP) lenses correct the irregular astigmatism of the anterior corneal surface in keratoconic eyes. However, residual refractive aberrations have been detected that are supposed to result from aberrations of the internal optics, that is, the lens and posterior corneal surface.[17–20]

The anterior and posterior corneal curvatures are affected in keratoconus.[21–23] The corneal aberrations calculated from the anterior surface may not be precise, because the contribution of the posterior surface to the corneal optical performance cannot be ignored.[24,25] Evaluating aberrations caused by the posterior corneal surface by analyzing posterior corneal topographic data obtained with a slit-scanning topographer will help to assess more precisely the deformed corneal optical performance.[26,27]

Zernike polynomial expansion has been one of the most useful methods to represent ocular HOAs. The usefulness of the simplified representation of the HOAs expressed as a Zernike vector term has been reported previously,[17,28,29] and allows an understanding of the relation between the anterior and posterior corneal aberrations.

In the present study, the corneal aberrations caused by the refraction on the anterior and posterior surfaces were evaluated separately. The aberrations were calculated from the anterior and posterior corneal heights and pachymetric data obtained with a rotating Scheimpflug camera and then expanded as Zernike vector terms to easily understand the relation between the anterior and posterior corneal aberrations.

Methods

Twenty-four normal control eyes of 24 normal control subjects and 28 keratoconic eyes of 24 patients were studied. The detailed characteristics of the subjects are shown in Table 1. The normal control eyes had no ocular disorders except for refractive errors. Only one eye of each control subject was used. The eyes with keratoconus were diagnosed by one experienced clinician (NM). The criteria for diagnosing keratoconus were the presence of central thinning of the cornea with a Fleischer ring, Vogt's striae, or both, by slit-lamp examination.[9] Eyes with forme fruste keratoconus were not included. Keratoconic eyes

Investigative Ophthalmology & Visual Science, June 2009, Vol. 50, No. 6

TABLE 1. Subject Data

	Controls	Keratoconus	*P*-value
No. cases/eyes	24/24	24/28	
Sex (male/female)	14/10	19/9	0.673*
Age, y (mean ± SD)	37.8 ± 14.2	35.5 ± 9.5	0.778†

* Chi-square test.
† Mann-Whitney rank sum test.

with corneal scarring and a history of acute hydrops or other disorders that affect topographic examinations were excluded.

The research adhered to the tenets of the Declaration of Helsinki. The Institutional Review Board of Osaka University approved this study. Informed consent was obtained from all participants after the purpose of the study and the procedures were explained.

The participants' eyes were examined using a rotating Scheimpflug camera (Pentacam; Oculus, Inc., Wetzlar, Germany). Twenty-five pictures were taken during one scan to reconstruct a three-dimensional model of the entire corneal configuration. All subjects were examined at least twice to confirm the reproducibility of the obtained data. The examination quality data were accessed with a built-in program, and the results with serious errors were excluded.

The rotating camera system (Pentacam; Oculus, Inc.) corrects distortions in the Scheimpflug images based on the geometry of the Scheimpflug principle and the refraction of the anterior surface to show various color-coded maps of anterior segment configurations, including corneal heights and pachymetric data. After this correction, the anterior and posterior corneal heights and pachymetric data of the subjects were exported to spreadsheet software (Excel 2000; Microsoft, Inc., Redmond, WA). These data consisted of numerical values of the anterior and posterior heights, the coordinates of the center of the pupil, and the corneal thickness in increments of 1 μm at the coronal plane and coordinates in increments of 0.1 mm. The HOAs of 6 mm pupils were calculated separately by an original program for the anterior and posterior corneal surfaces. The program expanded the anterior and posterior height data to Zernike polynomials and extracted the components of the ideal wavefront of the best-fit sphere. The aberrations were calculated by multiplying the residual components by the difference in the refractive indices on the anterior and posterior surfaces. The spherical aberrations included by the reference spherical body itself were added to avoid underestimation of the spherical aberrations. The refractive indices of the cornea and aqueous humor in the program were 1.376 and 1.336, respectively. The reference axes of the measurements were aligned with the primary line of sight according to the coordinates of the center of the pupil.

The wavefront aberration was expanded with the normalized Zernike polynomials. For each pair of the standard Zernike terms for trefoil, coma, tetrafoil, and secondary astigmatism, a combined value for the magnitude and axis was calculated by Zernike vector analysis. The detailed formulas to calculate this value for each term were reported previously.[17] In the present study, Zernike vector analysis was used to comprehend the relation between the anterior and posterior corneal aberrations. The axes of the left eyes were transposed about the vertical axis to correct for enantiomorphism of the right eyes.[30]

The averages of the magnitude and axis for each Zernike vector term were calculated by simple averaging of the magnitude and by vector calculation, similar to the well-known method for vector analysis of the cylinder.[17,31] Total HOAs were defined as the root mean square of the magnitudes for the third- and fourth-order aberrations. The magnitude of the spherical aberration was expressed as a positive or negative value and not as an absolute value. The axial range for each Zernike vector term varies according to each rotationally symmetric angle. Based on the ranges of the axis in Zernike vector terms, the angles were doubled in secondary astigmatism, tripled in trefoil, or quadrupled in tetrafoil during the calculation of the average magnitudes and axes in Zernike vector terms.

Data were analyzed using statistical analysis software (Sigma Stat ver. 2.0; SPSS, Inc., Chicago, IL). The χ^2 test was used to compare the sex ratio of the subjects. The Mann–Whitney rank sum test was used to compare the age and the radii of curvature of the anterior and posterior best-fit spheres between the keratoconus group and the control group and to compare the magnitude of the total HOAs, trefoil, coma, tetrafoil, secondary astigmatism, and spherical aberration due to the anterior and posterior corneal surfaces between both groups. $P < 0.05$ was considered significant.

RESULTS

There was no significant difference between the groups in age and sex (Table 1). Figure 1 shows the radii of curvature of the best-fit sphere used to calculate the HOAs for each surface. The means ± SD of the radii of the anterior and posterior best-fit spheres in keratoconic eyes (6.80 ± 0.74 mm and 5.18 ± 0.71 mm, respectively) were significantly shorter compared with control eyes (7.66 ± 0.40 mm and 6.25 ± 0.37 mm) for both corneal surfaces ($P < 0.001$, Mann–Whitney rank sum test).

Figure 2 shows the color-coded maps of the anterior and posterior corneal HOAs from a control eye and a typical keratoconic eye. Although no clinically relevant HOAs were detected in the control eye, an inferior slow pattern—that is, a pattern in which the slow wavefront area was inferior—was detected in the keratoconic eye for the HOAs of the anterior surface. The HOAs from the posterior surface were smaller in the opposite direction—a superior slow pattern— compared with the anterior surface.

Figure 3 shows the simple averages of the magnitudes of the total HOAs and each Zernike vector term for the 6 mm diameter. The means ± SD of the total HOAs due to the anterior and posterior surfaces in keratoconic eyes (4.34 ± 2.71 μm and 1.09 ± 0.66 μm, respectively) were significantly higher ($P < 0.001$, Mann–Whitney rank sum test) than those in control eyes (0.46 ± 0.26 μm and 0.15 ± 0.04 μm) for both corneal surfaces. The HOAs of the anterior surfaces were about three or four times larger than those of the posterior surfaces in both groups. The mean magnitudes of trefoil, coma, tetrafoil, and secondary astigmatism due to the anterior and posterior surfaces were also significantly higher ($P < 0.001$, Mann–Whitney rank sum test) in the keratoconic eyes than in the control eyes. The means ± SD of the spherical aberration due to the anterior

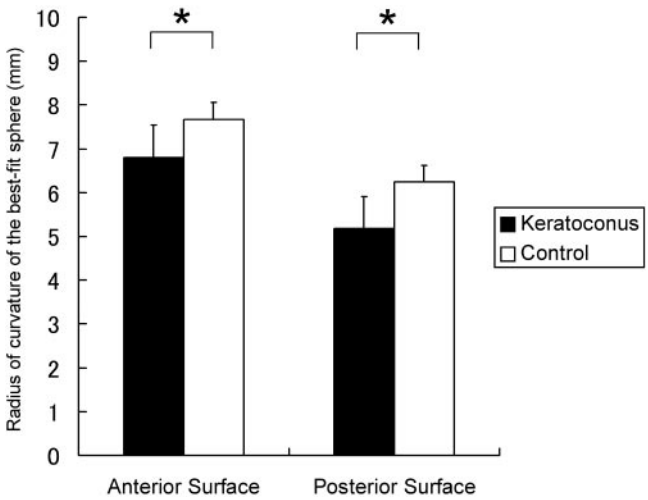

FIGURE 1. The radii of curvature of the best-fit sphere used to calculate HOAs for each surface. The radii of curvature of the best-fit sphere in keratoconic eyes are significantly shorter than those of control eyes for both corneal surfaces. *$P < 0.001$, Mann–Whitney rank sum test.

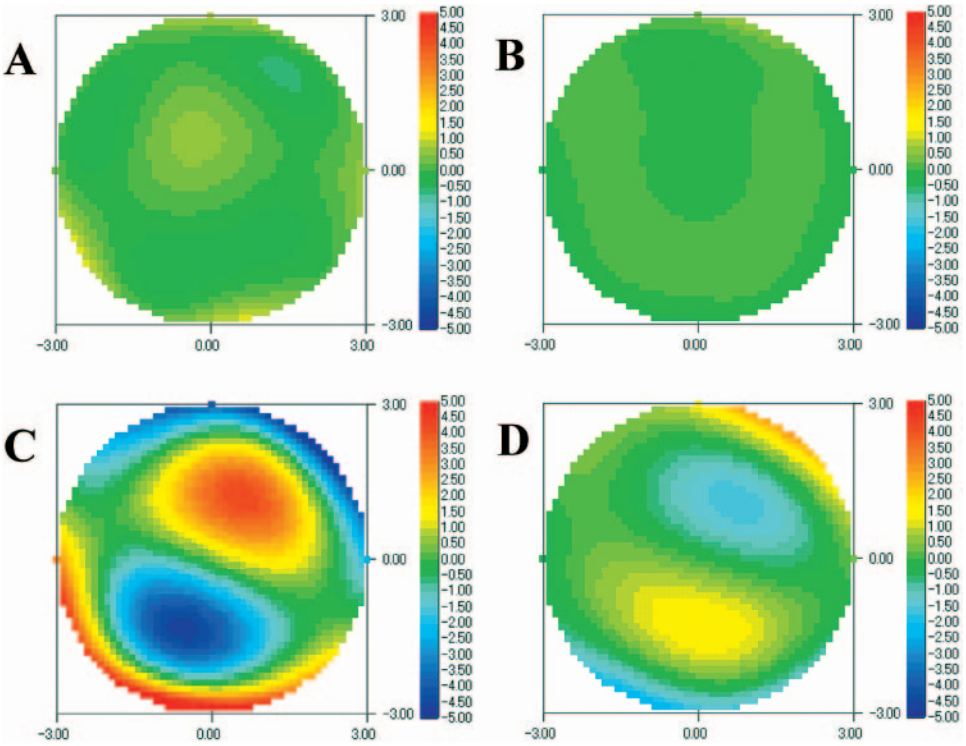

FIGURE 2. Aberration maps of HOAs due to the anterior/posterior corneal surfaces for a normal control eye (**A**, **B**) and a typical keratoconic eye (**C**, **D**). The HOAs from the posterior surface are smaller in the opposite direction than those from the anterior surface.

and posterior surfaces in keratoconic eyes (-0.44 ± 1.37 μm and 0.17 ± 0.40 μm) were significantly different ($P < 0.001$, $P = 0.002$, respectively, Mann–Whitney rank sum test) from those in the control eyes (0.25 ± 0.09 μm and -0.07 ± 0.04 μm) for both corneal surfaces.

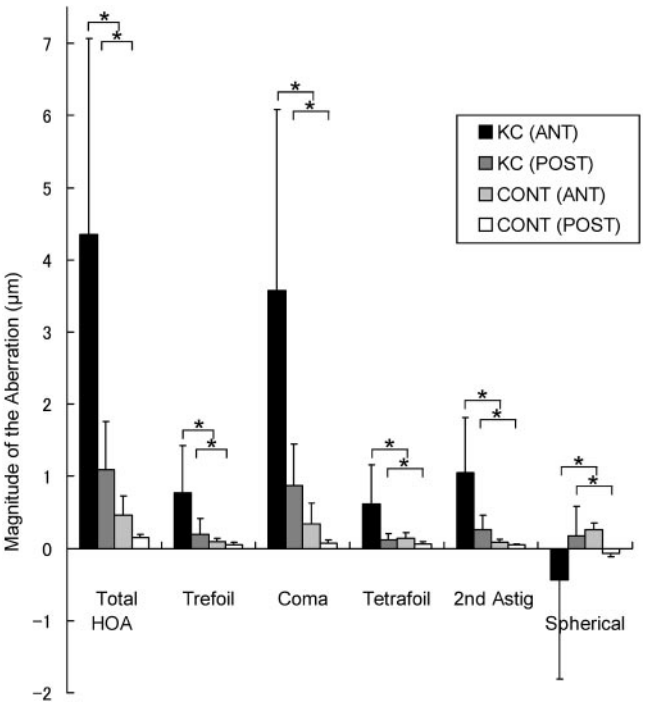

FIGURE 3. The graph shows the simple averages of the magnitudes of the total HOAs (RMS) and each Zernike vector term. The mean total HOAs, trefoil, coma, and spherical aberration due to the anterior and posterior surfaces are significantly higher in the keratoconic eyes than in normal control eyes. *$P < 0.001$, Mann–Whitney rank sum test. ANT, anterior surface; POST, posterior surface; KC, keratoconic eyes; CONT, control eyes; 2nd astig, secondary astigmatism.

Figure 4 shows the Zernike vector terms of trefoil, coma, tetrafoil, and secondary astigmatism due to the anterior and posterior surfaces on the polar coordinates. Regarding trefoil, the axes in most keratoconic eyes ranged from 60° to 120° for the anterior surface, but from 0° to 60° for the posterior surface. Regarding coma, the axes in many keratoconic eyes were distributed around 90° and in some from 45° to 90° for the anterior surface, but the axes were point symmetrically distributed from 180° to 270° for the posterior surface. For both trefoil and coma, the axes in the control eyes were evenly scattered for the anterior and posterior surfaces, and the orientations did not have apparent characteristics. For tetrafoil and secondary astigmatism, no apparent characteristics of the polar coordinates were observed.

Table 2 shows the results of vector calculation of the mean magnitude and axis of each Zernike vector terms for the anterior and posterior surfaces. The axes of coma for the anterior surface in keratoconic eyes (63.6°) and in control eyes (246.3°) were in opposite directions. The axes of trefoil, coma, tetrafoil, and secondary astigmatism for the anterior and posterior surfaces were in opposite directions according to each range of axes in the keratoconic eyes.

DISCUSSION

The main characteristic of the ocular and corneal HOAs in keratoconic eyes has been reported to be increased coma, especially vertical coma.[9,32] The present study also confirmed this pattern for the anterior corneal surface. We previously reported that Zernike vector analysis showed prominent vertical coma with an inferior slow pattern in keratoconic eyes,[17] and we also saw this pattern for the anterior corneal aberrations in the present study. The magnitude of the HOAs from the anterior surface cannot be directly compared with those for the entire cornea in the previous studies, because the refractive indices used to calculate the aberrations differed.

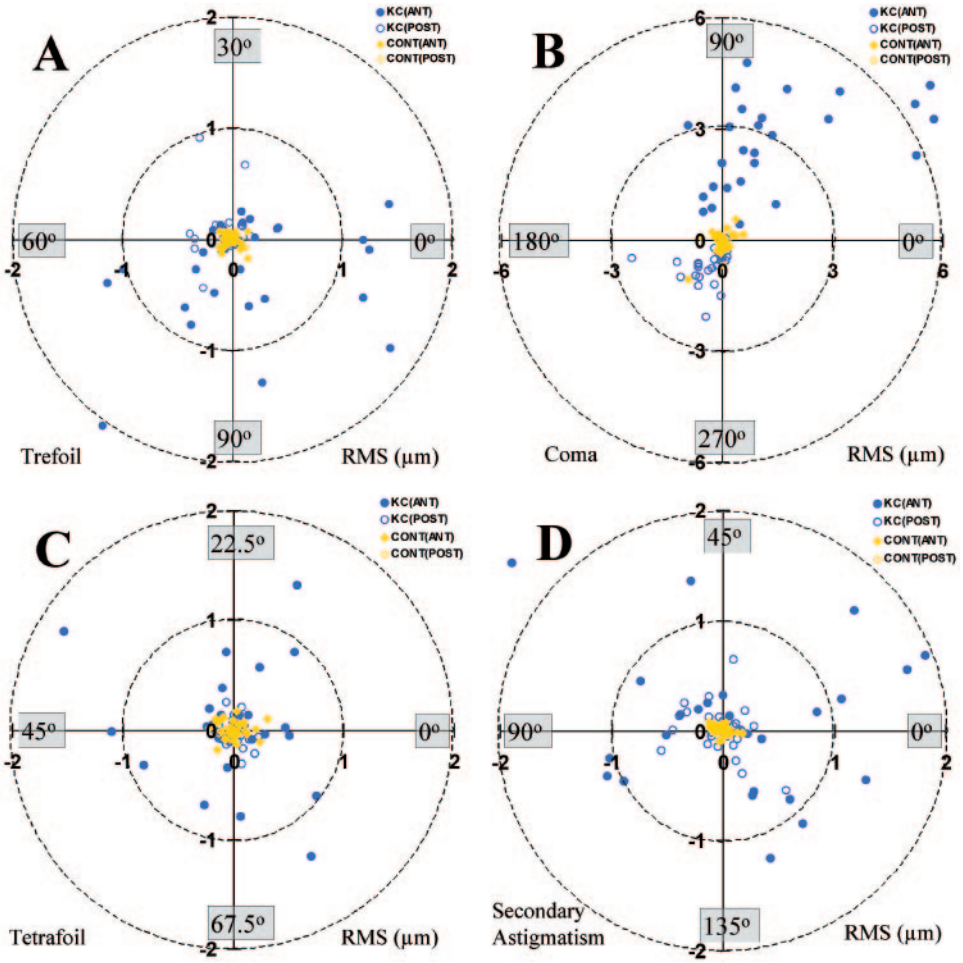

FIGURE 4. Scatterplots of trefoil (**A**), coma (**B**), tetrafoil (**C**), and secondary astigmatism (**D**) in the control and keratoconic eyes. The axes of the coma caused by the anterior and posterior surfaces are generally in opposite directions in the keratoconic eyes.

Although the keratometric index (1.3375) had been used to calculate the anticipated aberration for the entire cornea in our previous studies,[9,17] the refractive indices between the air (1.00) and the cornea (1.376) were used to calculate the corneal anterior aberrations in the present study.

The simple averages of the magnitudes of each Zernike vector term for the anterior surface were three or four times higher than those for the posterior surface. The greater difference in the refractive indices between the air and the cornea for the anterior surface compared with that between the cornea and the aqueous for the posterior surface probably caused these results. The vector calculation of the mean axis of each Zernike vector term for the anterior and posterior surfaces in the keratoconus group showed a mutually reverse pattern for trefoil, coma, tetrafoil, and secondary astigmatism. Increases in the refractive index at the anterior surface yield plus power, and decreases in the refractive index at the posterior surface induce minus power. This difference in the refractive indices and the similar pattern of the corneal configuration between the anterior and posterior surfaces probably caused these results.

The reverse pattern of each Zernike vector term due to the posterior corneal surface may play a role in compensating for the HOAs due to the anterior corneal surface in keratoconic eyes.[33] However, the precise HOAs of the entire cornea are not evaluated from the simple sum of these two, because the incident rays on the posterior surface have a deformed wavefront caused by refraction of the anterior surface. Dubbelman and colleagues reported that after refraction of the anterior surface, the wavefront that approached the posterior surface had the same form as the coma from the posterior surface.[27] Another study, using a virtual ray tracing based on the anterior and posterior surfaces, is needed to calculate more precisely the HOAs of the entire cornea and to evaluate the compensatory effect.[34]

In our previous study, the axes of ocular trefoil and coma were reversed in keratoconic eyes when a RGP lens was

TABLE 2. Vector Calculation of Mean Magnitude and Axis of Each Zernike Vector Term

Group	Trefoil	Coma	Tetrafoil	Secondary Astigmatism
Control				
Anterior surface	0.008@81.2	0.052@246.3	0.008@13.8	0.004@71.6
Posterior surface	0.017@79.7	0.016@293.9	0.010@57.5	0.002@25.9
Keratoconus				
Anterior surface	0.228@102.2	3.260@63.6	0.102@37.6	0.249@169.3
Posterior surface	0.094@46.8	0.779@241.9	0.024@82.9	0.032@92.5

worn.[17] The results of the present study strongly suggested that this reversal was caused mainly by the HOAs of the posterior surface when the RGP lens corrected the irregular astigmatism of the anterior corneal surface. The methods used in this study may enable prediction of the visual quality of a keratoconic eye with a RGP lens even before the lens is worn.

In the present study, we used the rotating camera system (Pentacam; Oculus, Inc.) to obtain a three-dimensional model of the shape of the entire cornea, because the central cornea, which can strongly affect the optical performance, was closely measured by the rotational imaging process. Placido ring-based videokeratography generally has good reproducibility because of rapid measurement, but it cannot measure the geometry of the corneal vertex or the posterior corneal surface. There is the potential for an artifact resulting from erroneously digitized narrowly spaced rings at steepening points in highly irregular corneas. Because there is little chance of this sort of artifact with the slit-scanning topographer, the corneal aberrations in keratoconic eyes with severe corneal protrusion may be evaluated more precisely with the slit-scanning topographer than by Placido ring-based videokeratography. However, movements of an eye being measured during scanning (1.0 seconds/25 scans) might affect the reliability of the obtained data. The rotating camera system can show corneal thickness and corneal curvature parameters, which also are calculated from the corneal height data. Previous studies have shown that the rotating camera (Pentacam; Oculus, Inc.) system provides measurements of central corneal thickness with good reproducibility and repeatability in not only normal eyes but also keratoconic eyes.[35,36] Other studies have reported that posterior and anterior corneal curvature parameters with the rotating camera (Pentacam; Oculus, Inc.) system were highly repeatable.[37,38] However, there also have been reports that the variability in the corneal elevation impaired corneal first-surface wavefront aberrations calculated using corneal topography (Pentacam; Oculus, Inc.).[39] Another study is needed to compare the HOAs from the posterior corneal surface measured according to a different principle.

The present study had some limitations. The effect of the refraction of the anterior surface on the Scheimpflug image was unavoidable, but it is difficult to prove the validity of the correction for these effects in an in vivo deformed cornea.[40–42] This problem would have to be solved to measure a deformed artificial model eye with a closed anterior chamber and the same refractive indices as a human cornea. We excluded patients with severe corneal opacities because the scattered scanning beam made it difficult to precisely digitize the corneal edges, and eyes with forme fruste keratoconus were not included. Another study is needed to determine whether the differences in the HOAs among normal eyes, eyes with forme fruste keratoconus, and eyes with clinical keratoconus could be shown. Measurement errors due to ocular movements during the examination cannot be prevented completely. High-speed three-dimensional anterior segment optical coherence tomography will solve these problems in the near future.[43,44] Smolek and Klyce and colleagues[45–47] reported that the Zernike polynomial fitting routine up to the tenth order caused loss of fine details with an abnormal corneal surface. Further evaluation of more Zernike terms is needed to improve the accuracy of the fitting of the HOAs.

We believe that evaluation of the aberrations due to the posterior corneal surface and Zernike vector analysis allows increased understanding of their characteristics and can be a useful method to assess the optical quality of keratoconic eyes and other corneal disorders. Because the curvature ratios of postoperative eyes between the anterior and posterior corneal surfaces differ from those in normal eyes,[48,49] evaluation of the corneal posterior aberrations also is needed after keratorefractive surgery or lamellar keratoplasty.

References

1. Krachmer JH, Feder RS, Belin MW. Keratoconus and related noninflammatory corneal thinning disorders. *Surv Ophthalmol.* 1984; 28:293–322.
2. Rabinowitz YS. Keratoconus. *Surv Ophthalmol.* 1998;42:297–319.
3. Maguire LJ, Bourne WM. Corneal topography of early keratoconus. *Am J Ophthalmol.* 1989;108:107–112.
4. Rabinowitz YS, McDonnell PJ. Computer-assisted corneal topography in keratoconus. *Refract Corneal Surg.* 1989;5:400–408.
5. Wilson SE, Lin DT, Klyce SD. Corneal topography of keratoconus. *Cornea.* 1991;10:2–8.
6. Maeda N, Klyce SD, Smolek MK, Thompson HW. Automated keratoconus screening with corneal topography analysis. *Invest Ophthalmol Vis Sci.* 1994;35:2749–2757.
7. Oshika T, Tomidokoro A, Maruo K, Tokunaga T, Miyata N. Quantitative evaluation of irregular astigmatism by Fourier series harmonic analysis of videokeratography data. *Invest Ophthalmol Vis Sci.* 1998;39:705–709.
8. Oshika T, Tanabe T, Tomidokoro A, Amano S. Progression of keratoconus assessed by Fourier analysis of videokeratography data. *Ophthalmology.* 2002;109:339–342.
9. Maeda N, Fujikado T, Kuroda T, et al. Wavefront aberrations measured with Hartmann-Shack sensor in patients with keratoconus. *Ophthalmology.* 2002;109:1996–2003.
10. Pantanelli S, MacRae S, Jeong TM, Yoon G. Characterizing the wave aberration in eyes with keratoconus or penetrating keratoplasty using a high-dynamic range wavefront sensor. *Ophthalmology.* 2007;114:2013–2021.
11. Langenbucher A, Gusek-Schneider GC, Kus MM, Huber D, Seitz B. Keratoconus screening with wave-front parameters based on topography height data. *Klin Monatsbl Augenheilkd.* 1999;214:217–223.
12. Schwiegerling J, Greivenkamp JE, Miller JM. Representation of videokeratoscopic height data with Zernike polynomials. *J Opt Soc Am A Opt Image Sci Vis.* 1995;12:2105–2113.
13. Schwiegerling J, Greivenkamp JE. Using corneal height maps and polynomial decomposition to determine corneal aberrations. *Optom Vis Sci.* 1997;74:906–916.
14. Applegate RA, Hilmantel G, Howland HC, Tu EY, Starck T, Zayac EJ. Corneal first surface optical aberrations and visual performance. *J Refract Surg.* 2000;16:507–514.
15. Alio JL, Shabayek MH. Corneal higher order aberrations: a method to grade keratoconus. *J Refract Surg.* 2006;22:539–545.
16. Buhren J, Kuhne C, Kohnen T. Defining subclinical keratoconus using corneal first-surface higher-order aberrations. *Am J Ophthalmol.* 2007;143:381–389.
17. Kosaki R, Maeda N, Bessho K, et al. Magnitude and orientation of Zernike terms in patients with keratoconus. *Invest Ophthalmol Vis Sci.* 2007;48:3062–3068.
18. Negishi K, Kumanomido T, Utsumi Y, Tsubota K. Effect of higher-order aberrations on visual function in keratoconic eyes with a rigid gas permeable contact lens. *Am J Ophthalmol.* 2007;144: 924–929.
19. Choi J, Wee WR, Lee JH, Kim MK. Changes of ocular higher order aberration in on- and off-eye of rigid gas permeable contact lenses. *Optom Vis Sci.* 2007;84:42–51.
20. Barbero S, Marcos S, Merayo-Lloves J. Corneal and total optical aberrations in a unilateral aphakic patient. *J Cataract Refract Surg.* 2002;28:1594–1600.
21. Tomidokoro A, Oshika T, Amano S, Higaki S, Maeda N, Miyata K. Changes in anterior and posterior corneal curvatures in keratoconus. *Ophthalmology.* 2000;107:1328–1332.
22. Tanabe T, Oshika T, Tomidokoro A, et al. Standardized color-coded scales for anterior and posterior elevation maps of scanning slit corneal topography. *Ophthalmology.* 2002;109:1298–1302.
23. Rao SN, Raviv T, Majmudar PA, Epstein RJ. Role of Orbscan II in screening keratoconus suspects before refractive corneal surgery. *Ophthalmology.* 2002;109:1642–1646.

24. Dubbelman M, Weeber HA, van der HeijdeRG, Volker-Dieben HJ. Radius and asphericity of the posterior corneal surface determined by corrected Scheimpflug photography. *Acta Ophthalmol Scand.* 2002;80:379–383.
25. Dubbelman M, Sicam VA, Van der Heijde GL. The shape of the anterior and posterior surface of the aging human cornea. *Vision Res.* 2006;46:993–1001.
26. Oshika T, Tomidokoro A, Tsuji H. Regular and irregular refractive powers of the front and back surfaces of the cornea. *Exp Eye Res.* 1998;67:443–447.
27. Dubbelman M, Sicam VA, van der Heijde RG. The contribution of the posterior surface to the coma aberration of the human cornea. *J Vis.* 2007;7:10.1–8.
28. Campbell CE. A new method for describing the aberrations of the eye using Zernike polynomials. *Optom Vis Sci.* 2003;80:79–83.
29. Oie Y, Maeda N, Kosaki R, et al. Characteristics of ocular higher-order aberrations in patients with pellucid marginal corneal degeneration. *J Cataract Refract Surg*. 2008;34:1928–1934.
30. Smolek MK, Klyce SD, Sarver EJ. Inattention to nonsuperimposable midline symmetry causes wavefront analysis error. *Arch Ophthalmol.* 2002;120:439–447.
31. Jaffe NS, Clayman HM. The pathophysiology of corneal astigmatism after cataract extraction. *Trans Am Acad Ophthalmol Otolaryngol.* 1975;79:OP615-OP630.
32. Schwiegerling J, Greivenkamp JE. Keratoconus detection based on videokeratoscopic height data. *Optom Vis Sci.* 1996;73:721–728.
33. Artal P, Guirao A, Berrio E, Williams DR. Compensation of corneal aberrations by the internal optics in the human eye. *J Vis.* 2001; 1:1–8.
34. Barbero S, Marcos S, Merayo-Lloves J, Moreno-Barriuso E. Validation of the estimation of corneal aberrations from videokeratography in keratoconus. *J Refract Surg.* 2002;18:263–270.
35. Amano S, Honda N, Amano Y, et al. Comparison of central corneal thickness measurements by rotating Scheimpflug camera, ultrasonic pachymetry, and scanning-slit corneal topography. *Ophthalmology.* 2006;113:937–941.
36. de Sanctis U, Missolungi A, Mutani B, Richiardi L, Grignolo FM. Reproducibility and repeatability of central corneal thickness measurement in keratoconus using the rotating Scheimpflug camera and ultrasound pachymetry. *Am J Ophthalmol.* 2007;144:712–718.
37. Chen D, Lam AK. Intrasession and intersession repeatability of the Pentacam system on posterior corneal assessment in the normal human eye. *J Cataract Refract Surg.* 2007;33:448–454.
38. Shankar H, Taranath D, Santhirathelagan CT, Pesudovs K. Anterior segment biometry with the Pentacam: comprehensive assessment of repeatability of automated measurements. *J Cataract Refract Surg.* 2008;34:103–113.
39. Shankar H, Taranath D, Santhirathelagan CT, Pesudovs K. Repeatability of corneal first-surface wavefront aberrations measured with Pentacam corneal topography. *J Cataract Refract Surg.* 2008; 34:727–734.
40. Koretz JE, Strenk SA, Strenk LM, Semmlow JL. Scheimpflug and high-resolution magnetic resonance imaging of the anterior segment: a comparative study. *J Opt Soc Am A Opt Image Sci Vis.* 2004;21:346–354.
41. Dubbelman M, van der Heijde RG, Weeber HA. Comment on "Scheimpflug and high-resolution magnetic resonance imaging of the anterior segment: a comparative study." *J Opt Soc Am A Opt Image Sci Vis.* 2005;22:1216–1218.
42. Dubbelman M, Van der Heijde GL, Weeber HA. Change in shape of the aging human crystalline lens with accommodation. *Vision Res.* 2005;45:117–132.
43. Sarunic MV, Asrani S, Izatt JA. Imaging the ocular anterior segment with real-time, full-range Fourier-domain optical coherence tomography. *Arch Ophthalmol.* 2008;126:537–542.
44. Miura M, Mori H, Watanabe Y, et al. Three-dimensional optical coherence tomography of granular corneal dystrophy. *Cornea.* 2007;26:373–374.
45. Smolek MK, Klyce SD. Zernike polynomial fitting fails to represent all visually significant corneal aberrations. *Invest Ophthalmol Vis Sci.* 2003;44:4676–4681.
46. Klyce SD, Karon MD, Smolek MK. Advantages and disadvantages of the Zernike expansion for representing wave aberration of the normal and aberrated eye. *J Refract Surg.* 2004;20:S537–541.
47. Smolek MK, Klyce SD. Goodness-of-prediction of Zernike polynomial fitting to corneal surfaces. *J Cataract Refract Surg.* 2005;31: 2350–2355.
48. Srivannaboon S, Reinstein DZ, Sutton HF, Holland SP. Accuracy of Orbscan total optical power maps in detecting refractive change after myopic laser in situ keratomileusis. *J Cataract Refract Surg.* 1999;25:1596–1599.
49. Sonego-Krone S, Lopez-Moreno G, Beaujon-Balbi OV, Arce CG, Schor P, Campos M. A direct method to measure the power of the central cornea after myopic laser in situ keratomileusis. *Arch Ophthalmol.* 2004;122:159–166.